the copper atoms, intrinsically possessing smaller N-Cu-N angles (i.e., tetrahedral vs trigonal), the stability of the boat conformer can be increased. A sample geometrical model in which all bond distances are kept constant and only the dihedral angle φ defined by the two pyrazolate rings is independently varied gives, for the N-Cu-N angle θ, the following expression:

$$\theta = \frac{180}{\pi} \cos^{-1}\left[\frac{b^2 + (a^2 - b^2)\cos(\phi\pi/180)}{a^2}\right] \quad (2)$$

where a and b are defined as the average observed Cu-N bond distance and the average projection of the Cu-N vectors onto the Cu···Cu hinge, respectively. Figure 3 shows the geometrical interpretation of this model and a plot of the θ vs φ function, from which it can be observed that small deviations from 120°, down to the observed θ values of 97.3 (1)°, 101.4 (1)° (compound **2**), 105.7 (2)°, and 107.7 (2)° (compound **3**) (see Tables IV and VI), can be obtained with much larger deviations from ideal coplanarity of the pyrazolate rings.

However, despite the geometric constraints imposed by the presence of stiff rings and of bond directionality in the donor nitrogen atoms of the pyrazolate ligands, a twisted (at first sight, unplausible) conformer in a highly sterically crowded coordination sphere of titanium atoms has been found in the $[(Cp)_2Ti(pz)]_2$ dimer.[22]

Acknowledgment. This research was supported by the Italian Consiglio Nazionale delle Ricerche (Progetto Finalizzato Chimica Fine II).

Registry No. **1**, 141344-55-0; **2**, 141344-56-1; **3**, 141344-57-2; $[Cu(CH_3CN)_4](BF_4)$, 15418-29-8.

Supplementary Material Available: A detailed list of crystallographic parameters (Table S1), full lists of bond distances and angles (Tables S2 and S3), lists of anisotropic thermal factors (Tables S4 and S5), and lists of hydrogen atom coordinates (Tables S6 and S7) (16 pages); lists of observed and calculated structure factor moduli (Tables S8 and S9) (44 pages). Ordering information is given on any current masthead page.

(22) Fieselman, B. F.; Sticky, G. D. *Inorg. Chem.* **1978**, *17*, 2074.

Contribution from the Discipline of Coordination Chemistry and Homogeneous Catalysis, Central Salt & Marine Chemicals Research Institute, Bhavnagar 364 002, India

Synthesis of the Monooxoruthenium(V) Complexes Containing the Amino Polycarboxylic Acid Ligands EDTA and PDTA and Their Reactivities in the Oxidation of Organic Substrates. X-ray Crystal Structures of $K[Ru^{III}(EDTA\text{-}H)Cl]\cdot 2H_2O$ and $K[Ru^{III}(PDTA\text{-}H)Cl]\cdot 0.5H_2O$

M. M. Taqui Khan,* Debabrata Chatterjee, R. R. Merchant, P. Paul, S. H. R. Abdi, D. Srinivas, M. R. H. Siddiqui, M. A. Moiz, M. M. Bhadbhade, and K. Venkatasubramanian

Received October 9, 1990

The syntheses and characterization of $K[Ru^{V}{=}O(EDTA)]$ (**3**) and $K[Ru^{V}{=}O(PDTA)]$ (**4**) are described. The kinetics of the formation of **3** and **4** by the interaction of the corresponding chloro complexes $K[Ru^{III}(EDTA\text{-}H)Cl]$ (**1**) and $K[Ru^{III}(PDTA\text{-}H)Cl]$ (**2**) with the oxygen atom donor NaOCl was investigated in the temperature range 30–50 °C. The activation parameters of the oxygenation reaction of **1** and **2** to **3** and **4**, respectively, are consistent with an associatively activated process. The O atom transfer reaction from **3** and **4** to the unsaturated and saturated hydrocarbons were studied spectrophotometrically in the temperature range 30–50 °C by following the disappearance of the characteristic oxo peak of the complexes at 393 nm and by product analysis. The activation parameters for the oxidation of the substrates corresponding to the rate-determining oxygen atom transfer step were determined, and a suitable mechanism was proposed. The crystal and molecular structures of the precursor complexes **1** and **2** were determined using single-crystal X-ray diffraction technique.

Introduction

Recently there has been an upsurge of interest in the ruthenium–oxo chemistry.[1-5] Many complexes containing Ru(IV)–oxo[1] and Ru(VI)–dioxo[2] moieties were reported and used as catalysts for the oxidation of a variety of organic compounds, including triphenylphosphine,[1a,b,2a] dimethyl sulfoxide,[1c] alcohols,[2a,b] phenols,[1d,e] olefins,[1a,b,2a,b] and alkanes.[2b,c,d,5] Ru(V)–oxo complexes were however comparatively less studied. The Ru(V)–oxo complex[3] $Ru^{V}{=}O(EDTA\text{-}H)$ catalyzes the oxidation of PPh_3 by molecular O_2. We have earlier studied[5,6] the formation of (μ-peroxo)ruthenium(IV) complexes with amino polycarboxylic acids and the catalysis of **1** in the oxidation of several organic substrates by molecular oxygen.[7,8]

The present investigation stems from our interest of developing new routes for the oxidation of saturated and unsaturated substrates catalyzed by $K[Ru^{III}(EDTA\text{-}H)Cl]$ (**1**) (EDTA-H = protonated ethylenediaminetetraacetate) and $K[Ru^{III}(PDTA\text{-}H)Cl]$ (**2**) (PDTA-H = protonated propylenediaminetetraacetate) in the presence of NaOCl as a cheap oxidant, which has successfully been used as an oxidant for the epoxidation of olefins by manganese porphyrins.[9,10] We report in this paper the kinetics

(1) (a) Moyer, B. A.; Slipe, B. K.; Meyer, T. J. *Inorg. Chem.* **1981**, *20*, 1475. (b) Che, C. M.; Wai, T.-T.; Lu, W.-O.; Wong, W.; Fong, L. T. *J. Chem. Soc., Dalton Trans.* **1989**, 2011. (c) Roecker, L.; Dobson, J. C.; Wing, W. J.; Meyer, T. G. *Inorg. Chem.* **1987**, *26*, 779. (d) Seok, W. K.; Meyer, T. J. *J. Am. Chem. Soc.* **1988**, *110*, 7358. (e) Seok, W. K.; Dobson, J. C.; Meyer, T. J. *Inorg. Chem.* **1988**, *27*, 3. (f) Dobson, J. C.; Seok, W. K.; Meyer, T. J. *Inorg. Chem.* **1986**, *25*, 1513.

(2) (a) Groves, J. T.; Quinn, R. J. *J. Am. Chem. Soc.* **1985**, *107*, 5790. (b) Che, C.-M.; Lai, T.-F.; Wong, K.-Y. *Inorg. Chem.* **1987**, *26*, 2289. (c) Bailey, C. L.; Drago, R. S. *J. Chem. Soc., Chem. Commun.* **1987**, 179. (d) Che, C.-M.; Leung, W.-H. *J. Chem. Soc., Chem. Commun.* **1987**, 1376. (e) Che, C.-M.; Wong, K.-Y. *J. Chem. Soc., Dalton Trans.* **1989**, 2065. (f) Amed, M.; Hendawy, E.; Griffith, W. P.; Taha, F. I.; Moussa, M. N. *J. Chem. Soc., Dalton Trans.* **1989**, 901.

(3) Taqui Khan, M. M.; Siddiqui, M. R. H.; Hussain, A.; Moiz, M. *Inorg. Chem.* **1986**, *25*, 2765.

(4) Dengel, A. C.; Griffith, W. P.; Maponey, C. A.; Williams, D. G. *J. Chem. Soc., Chem. Commun.* **1989**, 1720.

(5) Che, C.-M.; Vivian, W.-W. Y.; Mak, T. C. W. *J. Am. Chem. Soc.* **1990**, *112*, 2284.

(6) (a) Taqui Khan, M. M.; Ramachandraiah, G. *Inorg. Chem.* **1982**, *71*, 2109. (b) Taqui Khan, M. M. *Pure Appl. Chem.* **1983**, *55*, 159.

(7) Taqui Khan, M. M.; Hussain, A.; Subramanian, K. V.; Ramachandraiah, G. *J. Mol. Catal.* **1988**, *44*, 117.

(8) (a) Taqui Khan, M. M.; Shukla, R. S. *J. Mol. Catal.* **1986**, *34*, 19. (b) Taqui Khan, M. M.; Shukla, R. S. *J. Mol. Catal.* **1986**, *37*, 269. (c) Taqui Khan, M. M.; Shukla, R. S.; Rao, A. P. *J. Mol. Catal.* **1986**, *39*, 237. (d) Taqui Khan, M. M.; Shukla, R. S. *J. Mol. Catal.* **1989**, *39*, 139.

0020-1669/92/1331-2711$03.00/0

of the oxidation of **1** and **2** to the oxoruthenium(V) complexes $K[Ru^{V}{=}O(EDTA)]$ (**3**) and $K[Ru^{V}{=}O(PDTA)]$ (**4**) by NaOCl in water–dioxane medium. Complexes **3** and **4** were isolated and characterized on the basis of their elemental analysis and UV–vis, IR, CV, DPP, EPR, and magnetic susceptibility measurements.

The oxygen atom transfer from $[LRu^{V}{=}O]^{-}$ (L = EDTA, PDTA) to the olefins and saturated substrates was investigated by both spectrophotometric and product analysis methods in the temperature range 30–50 °C. The relative reactivities of the olefins toward epoxidation are explained in terms of the nucleophilicity and geometry of the olefins. The oxo complexes **3** and **4** are quite reactive in the insertion of the oxygen atom in the C–H bond to give alcohols except that tetrahydrofuran directly gave γ-butyrolactone. The reaction shows a large value of the kinetic isotope effect k_H/k_D in the case of cyclohexane (C_6H_{12}) and deuterated cyclohexane (C_6D_{12}) oxidation.

Experimental Section

Synthesis of Ruthenium Complexes. K[Ru(EDTA-H)Cl] (**1**) and K[Ru(PDTA-H)Cl] (**2**) were prepared from $K_2[RuCl_5(H_2O)]$ by following the published method.[11,12] Complexes **1** and **2** rapidly became aquated in aqueous solution to give the aquo complexes $[Ru^{III}(EDTA\text{-}H)(H_2O)]$ (**1a**) and $[Ru^{III}(PDTA\text{-}H)(H_2O)]$ (**2a**) at low pH.[13,14] Iodosylbenzene was prepared according to the literature procedure.[15] All other chemicals used were of AR grade. Double-distilled water and purified dioxane were used for preparing all the experimental solutions. A solution of NaOCl was purchased and titrated with standard thiosulfate solution[16] (1 mL of NaOCl was diluted to 10 mL with double-distilled water). The pH of the solution was 10.2. The purity of the NaOCl in a 5% solution was 80%, the remaining being NaCl; free Cl_2 was found in traces.

Synthesis of $L[Ru^{V}{=}O(EDTA)]\cdot 3H_2O$ and $K[Ru^{V}{=}O(PDTA)]\cdot 3H_2O$. To a solution (5 mL) of complexes **1**/**2** (1 mmol) was slowly added iodosylbenzene (1.1 mmol) dissolved in a minimum volume (10 mL) of 1:1 water–dioxane mixture. The reaction mixture was allowed to stir for 1 h (in the dark) at room temperature, and the PhI so formed was extracted by ether. The solution was concentrated at room temperature under vacuum to 2–3 mL. On addition of ethanol (8 mL) dropwise, a greenish-brown compound was precipitated. The precipitate was immediately filtered off, washed with alcohol, and dried under vacuum (yield 70% on the basis of complexes **1**/**2** taken; 63% on the basis of iodosylbenzene consumed).

The same compound can be prepared with NaOCl (in place of iodosylbenzene) at basic medium (pH ~ 9) in about 8 h of stirring (yield 72% on the basis of $LRu^{III}(H_2O)^{-}$ complexes taken; 64% on the basis of NaOCl used). This method was adapted for the synthesis of ^{18}O-labeled **3** and **4** by using $Na^{18}OCl$. Anal. Found (calcd) for $K[Ru^{V}{=}O(EDTA)]\cdot 3H_2O$ (**3**): C, 24.3 (24.1); H, 3.3 (3.6); N, 5.1 (5.6). Found (calcd) for $K[Ru^{V}{=}O(PDTA)]\cdot 3H_2O$ (**4**): C, 25.2 (25.8); H, 3.1 (3.9); N, 5.4 (5.5). Magnetic susceptibility at 298 K: $\mu_{eff}(3) = 1.98\ \mu_B$; $\mu_{eff}(4) = 2.03\ \mu_B$. Molar conductivity in water (Λ_M) at 298 K: $\Lambda_M(3) = 175\ \Omega^{-1}\ mol^{-1}\ cm^2$, $\Lambda_M(4) = 190\ \Omega^{-1}\ mol^{-1}\ cm^2$. Characteristic absorption peaks [λ_{max}, nm (ϵ_{max}, $mol^{-1}\ dm^3\ cm^{-1}$)]: **3**, 391 (8000 ± 20); **4**, 391 (7580 ± 30).

Instrumentation and Techniques. Microanalyses were carried out by the use of a Carlo Erba elemental analyzer. The electronic spectra of the complexes were recorded with a Shimadzu 160 UV–visible spectrophotometer. The IR and far-IR spectra were recorded on Beckman Acculab 10 (4000–600 cm^{-1}) and Perkin-Elmer 621 (600–200 cm^{-1}) spectrometers, respectively. The electrochemical studies were made with a Princeton Applied Research (PAR) instrument equipped with a Precision X-Y recorder. EPR studies were performed on a Bruker ESP 300 X-band spectrometer attached to an ESP 1600 data system and by using 100-kHz field modulation. The magnetic field was calibrated with the help of an ERO 35M NMR gaussmeter. Experiments were done on powdered samples at 298 K. Magnetic susceptibilities of complexes **3** and **4** were measured at room temperature (298 K) with a PAR 155 vibrating-sample magnetometer. A Digisun conductivity bridge was used for conductivity measurements. The pH measurements were carried out with a Digisun pH meter with an accuracy of ±0.01 unit.

Table I. Crystal Data

formula	$K[Ru(C_{11}H_{15}N_2O_8)Cl]\cdot 0.5H_2O$ (**2**)	$K[Ru(C_{10}H_{13}N_2O_8)Cl]\cdot 2H_2O$ (**1**)
mol wt	489.5	500.5
cryst system, space group	orthorhombic, *Pbcn*	monoclinic, $P2_1/c$
a, Å	13.537 (4)	19.460 (2)
b, Å	7.729 (1)	6.983 (1)
c, Å	31.973 (1)	12.679 (2)
β, deg		105.96 (1)
V, Å^3	3345.5 (1.2)	1656.5 (5.2)
Z	8	4
D_{calc}, g/cm^3	1.657	2.026
$F(000)$ abs, cm^{-1}	97.4	14.0
2θ range, deg	4–130	4–50
radiation (λ, Å)	Cu Kα (1.5418)	Mo Kα (0.7107)
temp, K	295	295
scan method	$\omega/2\theta$	$\omega/2\theta$
collcd octants	$+h,+k,\pm l$	$+h,+k,\pm l$
no. of data collcd	2835	2911
no. of data used, $\lvert F_{obs}\rvert > 3\sigma(\lvert F_{obs}\rvert)$	2093	2066
max–min transm factor	1.00–0.63	1.00–0.76
R	0.053	0.037
R_w	0.049	0.037

Kinetic Studies. The kinetics of oxygenation of $LRu^{III}(H_2O)^{-}$ (L = EDTA, PDTA) with NaOCl were studied spectrophotometrically by following the development of the characteristic absorption peaks of the respective oxo complexes **3** and **4** by using a Shimadzu 160 UV–visible spectrophotometer equipped with a TCC-240A temperature controller. The stoichiometric oxygen atom transfer from $LRu^{V}(O)^{-}$ to unsaturated and saturated hydrocarbons was studied spectrophotometrically by following the disappearance of the oxo peaks of the respective oxo complexes **3** and **4** at a constant pH 5.0 and ionic strength 0.1 M $NaClO_4$. For this purpose equal volumes of the $LRu^{V}(O)^{-}$ complex (2×10^{-4} M) and substrate of desired concentration (ranges from 2×10^{-3} to 2×10^{-2} M) were mixed in a spectrophotometric cell (before mixing, kinetic solutions were pre-equilibrated at the experimental temperature).

Product Analysis. Reaction products were identified by direct analysis of the reaction mixture using gas chromatography. A Shimadzu gas chromatograph (GC 9A) equipped with a stainless steel column containing 10% carbowax 20M on 90–100 mesh Anakrom working on TCD at 200 °C (N_2 carrier gas) was used for this purpose. Authentic samples of the oxidation products of the substrates were used for comparison of peak areas and corresponding retention times with the experimental products. For identification of reaction products of the oxidation of *cis*-stilbene and *trans*-stilbene, the reaction mixture was extracted with diethyl ether, and after solvent (ether) evaporation the residue was quantitatively transferred to an NMR tube using $CDCl_3$ as solvent. ^1H NMR spectra of the reaction products were recorded using TMS as an internal standard. A signal for the epoxidic proton for the cis isomer was found at δ 4.42 (singlet), and that at δ 3.87 (singlet) was for the trans isomer. A mixture of *cis*- and *trans*-epoxide was not obtained in any of the reactions involving oxidation of *cis*-stilbene or *trans*-stilbene. All the reaction products (principal products only) were further confirmed by ^{13}C NMR spectra recorded on a JEOL FX-100 NMR spectrometer.

X-ray Crystallographic Studies. Crystals of **1** and **2** suitable for X-ray studies were grown by slow evaporation of their aqueous solutions. Yellow platelike crystals of approximate dimensions 0.18 × 0.15 × 0.08 mm^3 was selected for **1**, and a similar crystal of dimensions 0.15 × 0.10 × 0.06 mm^3 was selected for **2**. Intensity data were collected on an Enraf-Nonius CAD-4 diffractometer using graphite-monochromatized Mo Kα radiation (λ = 0.7107 Å) for **1** and Cu Kα radiation (λ = 1.5418 Å) for **2**. In each case the accurate cell dimensions were determined from the least-squares refinement of 25 high-angle reflections.

Crystal stability and orientation during the entire period of data collection was monitored by periodically remeasuring three control reflections, which showed only statistical fluctuations. Intensities were corrected for Lorentz effects. (P7). Empirical absorption corrections[17] were applied to both data sets using three strong reflections near $\chi \approx 90°$

(9) Collman, J. P.; Brauman, J. I.; Meunier, B.; Hayashi, T.; Kodadek, T.; Raybuck, S. A. *J. Am. Chem. Soc.* **1985**, *107*, 2000.
(10) Meunier, B. *Gazz. Chim. Ital.* **1988**, *118*, 485.
(11) Diamentis, A. A.; Dubrawski, J. V. *Inorg. Chem.* **1981**, *20*, 1192.
(12) Taqui Khan, M. M.; Kumar, A.; Shirin, Z. *J. Chem. Res. Synop.* **1986**, 130.
(13) Matsubara, T.; Creutz, C. *Inorg. Chem.* **1979**, *18*, 1956.
(14) Bajaj, H. C.; Eldik, R. V. *Inorg. Chem.* **1988**, *27*, 4052.
(15) Lucas, H. J.; Kennedy, E. R. *Organic Synthesis*; Wiley: New York, 1972; Collect. Vol. III, pp 482.
(16) Vogel, A. E. *A Textbook of Quantitative Inorganic Analysis*; 3rd ed.; ELBS, Longmann: London, 1961; p 364.
(17) North, A. C. T.; Phillips, D. C.; Mathews, F. S. *Acta Crystallogr.* **1968**, *A24*, 351.

by the ψ-scan method. Crystal data for **1** and **2** are given in Table I.

Structure **1** was solved by the heavy-atom method. A difference Fourier map, phased on the position of the Ru atom, followed by a few rounds of least-squares refinement and difference Fourier calculations, gave positions of all the 25 non-H atoms including 2 water molecules. Full-matrix least-squares refinement of these, isotropic followed by anisotropic, using a modified unit-weighing scheme[18] with the Dunitz–Seiler factor[19] applied was carried out till convergence reached. A difference Fourier map calculated at this stage contained most of the H atoms; the rest were picked up in the subsequent difference maps at stereochemically reasonable positions. Final cycles of full-matrix least-squares refinement with all non-H atoms (anisotropic) and H atoms (isotropic, kept fixed) continuing with the same weighing scheme with the Dunitz–Seiler factor[19] applied converged to the final R value of 0.037 (R_w = 0.037). In the last cycle, the shift to esd ratio was less than 0.03, and the residual electron density in the final difference map was 0.67 e Å^{-3}.

Structure **2** was also solved by the heavy-atom method. A difference Fourier map based on the Ru atom position followed by a few cycles of least-squares refinement and difference Fourier calculations revealed the positions of all the 25 non-H atoms including a water molecule in the special position. A difference Fourier map computed at a stage when anisotropic refinement converged contained most of the H atoms. Those of the H atoms not located in this map were located in the subsequent difference maps at stereochemically reasonable positions. The final cycles of full-matrix least-squares refinement with the inclusion of H atoms (isotropic, kept fixed) continuing with the modified unit-weighing scheme[18] with the Dunitz–Seiler factor[19] applied gave the final R value of 0.053 (R_w = 0.049). In the last cycle, the shift to esd ratio was less than 0.03, and the residual electron density in the final difference map was 0.5 e Å^{-3}. All the computations were carried out using SDP software[20] available on PDP-11/73 computer from Enraf-Nonius, Delft, The Netherlands. The scattering factors were from ref 21. Listings of anisotropic thermal parameters and positional parameters for non-H atoms, positions of H atoms, and F_o/F_c values for both structures are deposited as supplementary material.

Results and Discussion

X-ray Structures of Precursor Complexes 1 and 2. An ORTEP view[22] of complexes **1** and **2** is shown in Figure 7a,b along with the numbering of atoms in the molecules. In both the structures, the ligands EDTA and PDTA are pentadentate, forming four chelate rings with one of the carboxylate arms free and the sixth position, trans to N1, occupied by the chloride Cl21. The Ru^{III} coordination structure is a distorted octahedron; for example, angles O14–Ru–N1 (82.0 (2)° in **1** and 81.7 (2)° in **2**) and O14–Ru–N4 (166.2 (1)° in **1** and 164.6 (2)° in **2**) are significantly reduced from ideal octahedral values among other bond angles containing a ruthenium atom. The distribution of bond angles is very similar in the two structures, and the average deviation in angles from the ideal octahedron is 5.33 (1)° for **1** and 5.12 (2)° for **2**. An important structural feature of the molecules is the Ru–Cl bond distances (2.358 (4) Å in **1** and 2.393 (2) Å in **2**), longer than typical Ru–Cl bond distances reported.[23] It is noteworthy that the Ru–N1 bond distances 2.043 (4) Å in **1** and 2.049 (5) Å in **2**, trans to the chloride Cl21, are significantly shorter than the Ru–N4 distances 2.114 (4) Å in **1** and 2.101 (5) Å in **2**, indicating a trans effect for N1. Ru–O distances vary from 2.007 (4) to 2.067 (4) Å in **1** and 2.007 (5)–2.049 (5) Å in **2**, the longest bond being the same (Ru–O14) in both structures.

The conformations of the EDTA and PDTA ligands bound to Ru(III) are very similar despite the presence of the extra methyl group C22 in the latter. The rings R1 (Ru–N1–C7–C8–O16) are planar in both structures whereas rings R2 (Ru–C9–C10–O18–N4) are in the envelope form with the envelope head atom N4 in **1** deviating by 0.466 (4) Å and in **2** deviating by 0.400 (5) Å from the least-squares plane through the rest of the ring atoms. Ring G (Ru–C5–C6–O14–Ni) is also an envelope but much more puckered than the R2 rings. The deviation of N1 from the least-squares plane through the rest of the ring atoms is 0.639 (4) Å in **1** and 0.570 (5) Å in **2**. This ring is more strained than the R rings.[24]

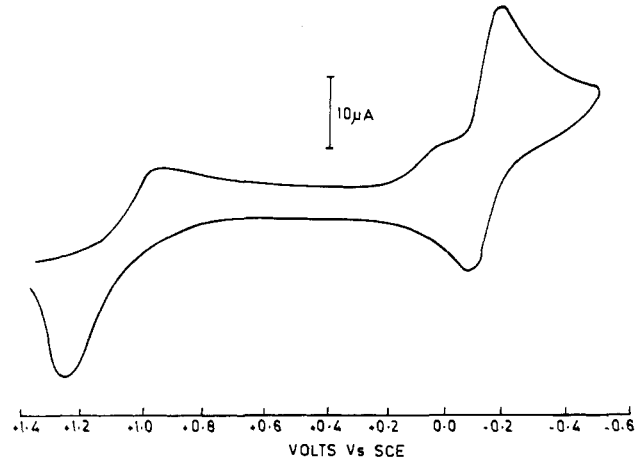

Figure 1. Cyclic voltammogram (CV) of complex **3** in 0.1 M $HClO_4$ medium at pH = 1.0 (glassy carbon working electrode; scan rate = 50 mV/s).

Characterization of Complexes 3 and 4. Complexes K[Ru=O(EDTA)] (**3**) and K[Ru^V=O(PDTA)] (**4**) are quite stable in the solid state and in aqueous solution at least for 1 week at room temperature. The greenish-brown solid complexes **3** and **4** were characterized by elemental analysis and UV–vis, IR, EPR, electrochemical, and magnetic susceptibility studies. The electronic spectra of complexes **3** and **4** show characteristic bands at λ/nm (ϵ_{max}/dm^3 mol^{-1} cm^{-1}) 391 (8000) and 393 (7500), respectively. These characteristic oxo bands are assigned to $\pi^*(O) \rightarrow t_{2g}Ru^V$ charge transfer in the oxo complexes. The IR spectra of complexes **3** and **4** (solid samples) show a peak at 890 cm^{-1} corresponding to the ν(Ru=O) stretch. The peaks are observed at 850 cm^{-1} in the ^{18}O-substituted complexes Ru^V=^{18}OL. The position of the band agrees with those reported for other Ru^V=O complexes, [Ru^V=O(O_2COCEt_2)$_2$]$^-$[4] at 900 cm^{-1} and [Ru^V=O(N_4O)]$^{2+}$ (N_4O = polydentate pyridylamine ligand)[5] at 872 cm^{-1}. The carboxyl region of the spectra shows a sharp band at 1720 cm^{-1} assigned to the uncoordinated carboxylate[25] group and a strong broad band around 1630–1640 cm^{-1} for coordinated carboxylate groups. The far-infrared spectra of the oxo complexes exhibit peaks around 330 and 410 cm^{-1} assigned to ν(Ru–N) and ν(Ru–O), respectively. The absence of any band around the 370–290-cm^{-1} region confirms the complete removal of chloride ion from the coordination sphere of L–Ru–Cl by the oxo group.

The cyclic voltammograms (CV) of the oxo complexes **3** and **4** taken in a 0.1 M $HClO_4$ medium at pH 1.0 with a glassy-carbon electrode give $E_{1/2}$ values vs SCE for Ru^{5+}/Ru^{4+} at +0.99 V for **3** and 0.98 V for **4**, Ru^{4+}/Ru^{3+} at +0.10 V for **3** and 0.20 V for **4**, and Ru^{3+}/Ru^{2+} at −0.17 V for **3** and −0.24 V for **4**. The $E_{1/2}$ values are nearly constant at different scan rates (10–100 mV s^{-1}) (Figure 1 for complex **3**). For the complex [Ru^V=O(N_4O)]$^{2+}$ $E_{1/2}$ at pH 1–3 for Ru^V/Ru^{III} was observed[5] at 1.02 V and that for Ru^{III}/Ru^{II} was observed at 0.35 V. The more positive potentials in the polypyridine complex are expected on the basis of a greater d_π–p_π interaction of the ligand as compared to the amino polycarboxylic acids that are σ-donors in complexes **3** and **4**. The Ru^{III}/Ru^{II} potentials in the Ru(IV)–oxo complexes observed by Meyer et al.[26] are also much more positive (0.52 V) as compared

(18) w = 1.0 for FOBS and THRES. w = (THRES/FOBS)^2 for FOBS and THRES; THRES is 80% of the largest FOBS.
(19) Dunitz, J. D.; Seiler, P. *Acta Crystallogr.* **1973**, *B29*, 589.
(20) Frenz, B. A. and Associates, College Station, TX, and Enraf-Nonius, Delft, Holland, Structure Determination Package, available on the PDP-11/73 computer.
(21) *International Tables for X-ray Crystallography*; Kynoch Press: Birmingham, England, 1974; Vol. IV, pp 71–102 (present distributor Kluwer Academic Publishers, Dordrecht, The Netherlands).
(22) Johnson, C. K. ORTEP II. Fortran Thermal-Elipsoid Plot Program for Crystal Structure Illustrations. Oak Ridge National Laboratory, March 1976.
(23) Bits, J. W.; Pandey, K. K.; Roesky, H. W. *J. Chem. Soc., Dalton Trans.* **1984**, 2081.
(24) Weakliem, H. A.; Hoard, J. L. *J. Am. Chem. Soc.* **1959**, *81*, 549.
(25) Nakamoto, K. *Infrared Spectra of Inorganic and Coordination Compounds*; Wiley: New York, 1970.
(26) Dobson, J. C.; Meyer, T. J. *Inorg. Chem.* **1988**, *29*, 3283.

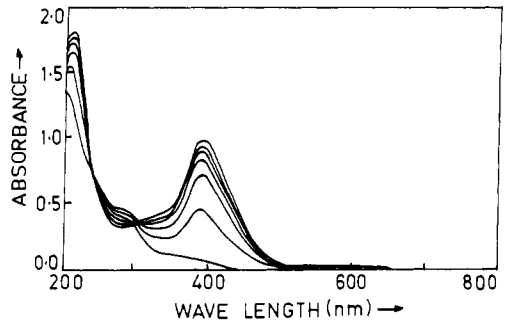

Figure 2. Development of the characteristic oxo peak (393 nm) of complex **3** at 30 °C.

to the same potentials in complexes **3** and **4**.

The magnetic susceptibility measurements have shown that Ru(V)–oxo complexes **3** and **4** are paramagnetic. The paramagnetism is slightly higher than one unpaired spin $S = {}^1/_2$ system due to orbital contribution to the magnetic moment. A μ_{eff} value of 2.2 μ_B was observed for the complex $[Ru^V{=}O(N_4O^{2+}]$.[5]

The EPR spectra of complexes **3** and **4** as powder samples at 298 K consist of a single broad line centered at $g = 2.218$ for complex **3** and $g = 2.205$ for complex **4**. The EPR spectral features are characteristic of a single unpaired electron ($S = {}^1/_2$) in a spin-paired ground-state electronic configuration $(t_{2g})^3$ of Ru(V).

The EPR reports on Ru(V) species are scarce. The complex tetra-*n*-propylammonium bis(2-hydroxy-2-ethylbutyrato)oxoruthenate(V), $(Pr^n{}_4N)[RuO(O_2COCEt_2)_2]$, with a trigonal bipyramidal geometry at the ruthenium site showed[27] a single EPR resonance in the solid state at $g = 1.986$. The higher g values observed in the present case, where ruthenium has an octahedral ligand coordination, could not be attributed to the admixture of a singlet ground state with the excited states via spin–orbit coupling interaction ($\lambda\vec{L}\cdot\vec{S}$). Apart from substantiating the formation of Ru(V)–oxo complexes, the magnetic moment and EPR studies indicate the ground-state electronic structure of ruthenium in these $Ru^V{=}O$ complexes as $d_{xy}{}^2d^1(\lambda^*)$ ($d^1 = d_{xz}, d_{yz}$).

The EPR spectra of the parent complexes **1** and **2** at 298 K as powder samples are characterized by rhombic **g** tensors with g components being 2.393 (6), 2.345 (6), and 1.765 (6) for **1** and 2.730 (6), 2.361 (6), and 1.409 (6) for **2**, corresponding to a distorted octahedral geometry around ruthenium as revealed by the X-ray studies and a $d_{xz}{}^2d_{yz}{}^2d_{xy}{}^1$ ground-state electronic configuration. It is obvious from the EPR data on complexes **1**–**4** that there is no rearrangement in the geometry of the original complexes **1** and **2** as regard to the ligation of EDTA and PDTA, with the only difference being that Cl^- in **1** and **2** is replaced by the oxo oxygen in **3** and **4**.

Kinetics of Oxygenation of $[LRu^{III}(H_2O)]^-$ to $[LRu^V{=}O]^-$ with NaOCl. The kinetics of oxygenation of complexes **1** and **2** were studied spectrophotometrically by following the buildup of the oxo peak (Figure 2) of the complexes **3** and **4**. The rate of reaction was found to be first order with respect to total Ru^{III}–EDTA concentration and total oxidant ($HOCl + OCl^-$) concentration. The rate was unaffected by an increasing in Cl^- concentration (0.1–0.3 M) in the system. But at very high Cl^- concentration (2 M), a marked decrease in rate ($k_4 = 0.82 \times 10^{-2}$ M^{-1} s^{-1}) was observed. This is due to the formation of the $(EDTA)Ru^{III}Cl^{2-}$ species, which was found to be less reactive toward substitution than corresponding aquo/hydroxo species.[28] The rate of reaction was found to decrease slowly with the increase in pH in the range 5.5–6.5. There is a sharp decrease in the rate in the pH range 7.0–8.0 (Figure 3) followed by an almost limiting value in the pH range 8.0–9.5. On the basis of the above kinetic observation (neglecting the other species produced in NaOCl solution at low

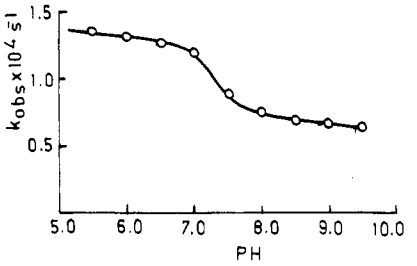

Figure 3. Effect of pH on the rate of oxygenation of complex **1** with OCl^- at 30 °C and ionic strength 0.1 M (KCl).

pH), a working mechanism for the oxidation of $(EDTA)Ru^{III}(H_2O)^-$ to $(EDTA)Ru^V(O)^-$ with sodium hypochlorite has been proposed in Scheme I.

Scheme I

$$\text{I}\quad Ru^{III}(EDTA)(H_2O)^- \overset{K_1}{\rightleftharpoons} Ru^{III}(EDTA)(OH)^{2-} + H^+ \quad (1)$$

$$pK_1 = 7.6$$

$$\text{II}\quad HOCl \overset{K_2}{\rightleftharpoons} OCl^- + H^+ \quad (2)$$

$$pK_2 = 7.5$$

$$\text{III}\quad Ru^{III}(EDTA)(H_2O)^- + HOCl \xrightarrow{k_1} \underset{A}{Ru^{III}(EDTA)(HOCl)^-} + H_2O \quad (3)$$

$$Ru^{III}(EDTA)(HOCl)^- \xrightarrow{fast} Ru^V(EDTA)(O)^- + H^+ + Cl^- \quad (4)$$

$$\text{IV}\quad Ru^{III}(EDTA)(H_2O)^- + OCl^- \xrightarrow{k_2} \underset{B}{Ru^{III}(EDTA)(OCl)^{2-}} + H_2O \quad (5)$$

$$Ru^{III}(EDTA)(OCl)^{2-} \xrightarrow{fast} Ru^V(EDTA)(O)^- + Cl^- \quad (6)$$

$$\text{V}\quad Ru^{III}(EDTA)(OH)^{2-} + HOCl \xrightarrow{k_3} \underset{C}{Ru^{III}(EDTA)(HOCl)^-} + OH^- \quad (7)$$

$$Ru^{III}(EDTA)(HOCl)^- \xrightarrow{fast} Ru^V(EDTA)(O)^- + H^+ + Cl^- \quad (8)$$

$$\text{VI}\quad Ru^{III}(EDTA)(OH)^{2-} + OCl^- \xrightarrow{k_4} \underset{D}{Ru^{III}(EDTA)(OCl)^{2-}} + OH^- \quad (9)$$

$$Ru^{III}(EDTA)(OCl)^{2-} \xrightarrow{fast} Ru^V(EDTA)(O)^- + Cl^- \quad (10)$$

On the basis of the above scheme, a rate expression can be derived for the oxygenation process

$$\text{rate} = \frac{k_1[H^+]^2 + (k_2K_2 + k_3K_1)[H^+] + k_4K_1K_2}{[H^+]^2 + (K_1 + K_2)[H^+] + K_1K_2}[Ru^{III}]_T[HOCl]_T \quad (11)$$

At low pH (~6) $[H^+] \gg K_1K_2$, (11) reduces to

$$\text{rate} = k_1[Ru^{III}]_T[HOCl]_T \quad (12)$$

from which k_1 is calculated as 1.15×10^{-1} M^{-1} s^{-1}. Similarly at high pH (~9), where $K_1K_2 \gg [H^+]$, (11) is reduced to

$$\text{rate} = k_4[Ru^{III}]_T[OCl^-] \quad (13)$$

from which k_4 is deduced as 0.71×10^{-1} M^{-1} s^{-1}. In the intermediate pH range 7–8, which is an inflection region for the dissociation of complex $[Ru^{III}(EDTA)(H_2O)]^-$ and HOCl, k_2 and k_3 are calculated by solving a set of simultaneous equations with known values of k_1, k_4, $[H^+]$, and K_1 and K_2. The values of k_2

(27) Dengel, A. C.; Griffith, W. P.; O'Mahoney, C. N.; Williams, D. J. *J. Chem. Soc., Chem. Commun.* **1989**, 1720.
(28) Taqui Khan, M. M.; Bajaj, H. C.; Chatterjee, D. *Indian J. Chem. A.* **1992**, *31*, 152.

Table II. Rate and Activation Parameters for the Oxidation of $LRu^{III}(OH)^{2-}$ to $LRu^{V}(O)^{-}$ with OCl^{-} at pH 9.0 and Ionic Strength 0.1 M (KCl)

system	temp, °C	$10k_4$, M^{-1} s^{-1}	$\Delta H^{\ddagger}$,[a] kcal/deg	$\Delta S^{\ddagger}$,[a] cal/(deg·mol)
$Ru^{III}(EDTA)(OH)^{2-}/OCl^{-}$	30	0.72		
	40	1.96	17	−7
	50	4.45		
$Ru^{III}(PDTA)(OH)^{2-}/OCl^{-}$	30	0.69		
	40	1.87	19	−7
	50	4.21		

[a] $\Delta H^{\ddagger}$ correct to ±1 kcal/mol. $\Delta S^{\ddagger}$ correct to ±1 eu.

Scheme II

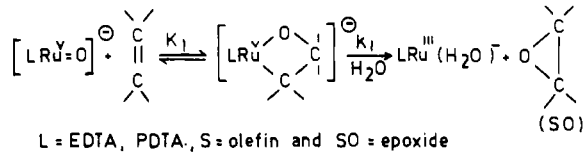

and k_3 are 0.97×10^{-1} and 0.83×10^{-1} M^{-1} s^{-1}, respectively. The formation of intermediate mixed-ligand complexes species A–D is suggested on the basis of the independence of the rate on Cl^{-} concentration. The evidence for the formation of A–D is thus indirectly based on kinetic observations. Similar kinetic behavior was observed for PDTA complex **2**. The formation of oxo complexes **3** and **4** was studied at three different temperatures. The rate and activation parameters corresponding to the step VI in Scheme I are summarized in Table II. The low values of $\Delta H^{\ddagger}$ and negative values of $\Delta S^{\ddagger}$ clearly support the proposed mechanism.

Kinetics of Oxygen Atom Transfer from $LRu^{V}(O)^{-}$ to Olefins. The kinetics of oxygen atom transfer from $LRu^{V}(O)^{-}$ to olefins, i.e. epoxidation of olefins, was investigated spectrophotometrically by following the disappearance of the characteristic oxo peaks of the respective oxoruthenium(V) complexes **3** and **4** at a fixed pH 5.0 and ionic strength of 0.1 M $NaClO_4$ in 1:1 water–dioxane medium. Under pseudo-first-order conditions of excess substrate (olefin) concentration, the rate of oxygen transfer was found to be first-order with respect to $LRu^{V}{=}(O)^{-}$ concentration. The observed rate constant depends on the olefin concentration, and a limiting rate is attained at high olefin concentration. One such dependence of observed rate constant on olefin concentration is depicted in Figure 4. The observed saturation in the reaction rate at high olefin concentration can be interpreted in terms of the mechanism outlined in Scheme II, for which a modified Michaelis–Menten rate expression is given in (14) and (15).

$$k_{1(obs)} = \frac{k_1 K_1 [S]}{1 + K_1 [S]} \tag{14}$$

$$\frac{1}{k_{1(obs)}} = \frac{1}{k_1} + \frac{1}{k_1 K_1 [S]} \tag{15}$$

In the proposed mechanism it is assumed that oxoruthenium(V) complexes $[LRu^{V}(O)^{-}]$ first react with olefins to produce a reactive intermediate I (Scheme II) in a rapid pre-equilibrium step. The oxygen atom transfer from the ruthenium center to olefins occurs in a subsequent rate-determining step.

The formation of a metallacyclooxetane intermediate

was earlier proposed in the oxygenation of olefins by manganese(III)[9,10] porphyrins by a 2 + 2 cycloaddition reaction. A concerted elimination of the epoxide gives back the Fe(III) catalyst. Radical carbon intermediate[29] M–O–C–C^{+} and radical ion-pair intermediates[30] were later proposed to account for the

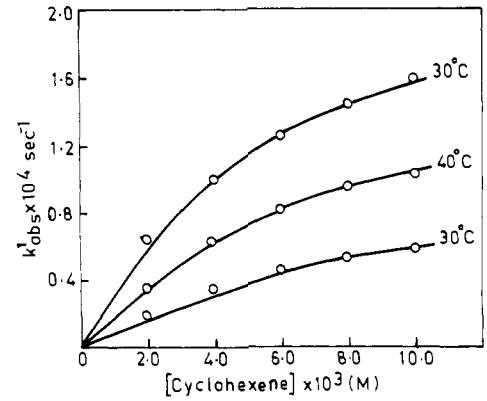

Figure 4. Dependence of observed rate constant ($k_{1(obs)}$) on [cyclohexene] at different temperatures.

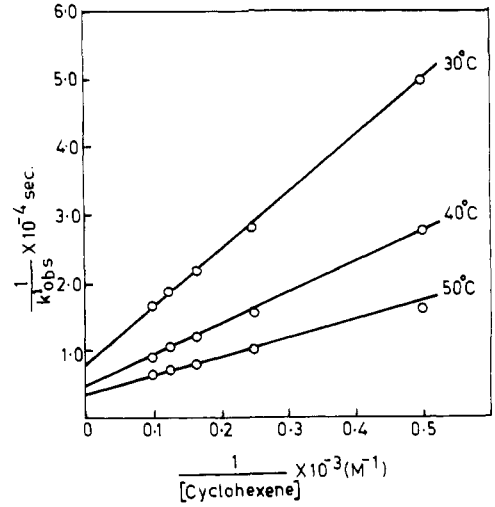

Figure 5. Plot of $k_{1(obs)}^{-1}$ versus $[cyclohexene]^{-1}$ at different temperatures.

reactivity of sterically encumbered olefins. In the latter case, the intermediate rearranges[30] by a spin-flop mechanism either to a metallacyclooxetane and the epoxide or an N-alkylated product; σ-bonded metalloporphyrins were also suggested as intermediates[31] in the epoxidation of 5,5-dimethylpentene. Drago[32] has calculated the probability of the various pathways for O atom transfer to olefins and has concluded that the formation of an oxo metallacycle either by a concerted or a nonconcerted 2 + 2 cycloaddition of olefin to Ru=O is unfavorable. His calculations have supported a 1 + 2 cycloaddition where only one carbon center of the olefin reacts with an oxo O atom to form a CO center followed by the combination of the other C atom to the electron-rich CO center.

Though we have proposed a metallacyclooxetane intermediate in our mechanism, it is only based on the formation of epoxides as the main product, with good stereoselectivity (i.e. *cis*-stilbene oxide from *cis*-stilbene and *trans*-stilbene oxide from *trans*-stilbene). Radical cation intermediates or radical ion-pair intermediates always give small quantities of rearranged products, which were not detected in our case.

At high olefin concentration a limiting rate was observed due to saturation of intermediate I with substrate. Further increase in concentration of olefins only changes its bulk concentration without affecting the rate of epoxidation. Plots of $1/k_{1(obs)}$ vs $1/[S]$ (eq 15) were linear in all cases, and one such plot is depicted in Figure 5. The values of k_2 (calculated from intercepts of the plots) at different temperatures are summarized in Table III.

The epoxidation reaction was studied at three different temperatures, and the activation parameters $\Delta H^{\ddagger}$ and $\Delta S^{\ddagger}$ calculated with the help of the Eyring equation are presented in Table III.

(29) Castellino, A. J.; Bruice, T. C. *J. Am. Chem. Soc.* **1988**, *110*, 1313.
(30) Ostovic, D.; Bruice, T. C. *J. Am. Chem. Soc.* **1989**, *111*, 6511.
(31) Dolphin, D.; Matsumoto, A.; Shortman, C. *J. Am. Chem. Soc.* **1989**, *111*, 411.
(32) Cundari, T. R.; Drago, R. S. *Inorg. Chem.* **1990**, *29*, 487.

Table III. Rate and Activation Parameters for the Reaction $LRu^{V}(O)^{-} + S \xrightarrow{k_{ox}} LRu^{III}(H_2O)^{-} + SO$ at pH 6.0 and I = 0.2 M ($NaClO_4$) in 1:1 Water–Dioxan Medium (L = EDTA, PDTA; S = Olefins and Saturated Hydrocarbons, $[Ru^{V}] = 1 \times 10^{-4}$ M; [S] = 2×10^{-3}–2×10^{-2} M)

	$(EDTA)Ru^{V}(O)^{-} + S \xrightarrow{k_{ox}} (EDTA)Ru^{III}(H_2O)^{-} + SO$				$(PDTA)Ru^{V}(O)^{-} + S \xrightarrow{k_{ox}} (PDTA)Ru^{III})H_2O) + SO$			
S	temp, °C	10^4k, s^{-1}	$\Delta H^{\ddagger}$, kcal/mol	$\Delta S^{\ddagger}$, cal/(deg mol)	temp, °C	$10^4k'$ s^{-1}	$\Delta H^{\ddagger}$,[a] kcal/mol	$\Delta S^{\ddagger}$,[b] cal/(deg mol)
cyclohexene	30	1.25	8	−30	30	1.33	7	−51
	40	1.94			40	2.22		
	50	2.98			50	3.12		
cyclooctene	30	1.66	7	−52	30	1.71	7	52
	40	2.44			40	2.56		
	50	3.68			50	3.80		
styrene	30	0.62	9	−49	30	0.73	8	50
	40	1.01			40	1.17		
	50	1.63			50	1.82		
cis-stilbene	30	0.48	10	−45	30	0.60	9	−48
	40	0.83			40	1.02		
	50	1.43			50	1.63		
trans-stilbene	30	0.36	12	−39	30	0.43	11	41
	40	0.66			40	0.79		
	50	1.33			50	1.40		
cyclohexane	30	0.052	8	−55	30	0.062	8	−56
	40	0.082			40	0.098		
	50	0.133			50	0.150		
tetrahydrofuran	30	0.074	6	−62	30	0.090	5	−64
	40	0.100			40	0.120		
	50	0.154			50	0.162		
2-Me-styrene	30	0.75	8	−52	30	0.81	7	−53
	40	1.23			40	1.29		
	50	1.75			50	1.91		
3-Cl-styrene	30	0.48	9	−48	30	0.52	9	−48
	40	0.82			40	0.87		
	50	1.32			50	1.39		
4-MeO-styrene	10	0.37	6	−56	10	0.41	6	−50
	20	0.56			20	0.62		
	30	0.82			30	0.82		
cyclohexanol	30	0.09	6	−62	30	0.10	6	−63
	40	0.13			40	0.14		
	50	0.18			50	0.19		
benzyl alcohol	30	0.40	5	−63	30	0.43	5	−64
	40	0.52			40	0.60		
	50	0.70			50	0.75		

[a] $\Delta H^{\ddagger}$ accurate to ±1 kcal/mol. [b] $\Delta S^{\ddagger}$ accurate to ±11 eu.

Table IV. Oxidation of Unsaturated and Saturated Organic Compounds by $LRu^{V}(O)^{-}$ (L = EDTA) at 30 °C in Water–Dioxane Medium ($[Ru^{V}]$ = 1 mM; [Substrate] = 1 mM)

substrate	product	yield[a] (η),[b] %
cyclohexene	cyclohexene oxide	53
cyclooctene	cyclooctene oxide	60
styrene	styrene oxide	47
	phenylacetadehyde	<1
2-Me-styrene	2-Me-styrene oxide	51
3-Cl-styrene	3-Cl-styrene oxide	35
4-MeO-styrene	4-MeO-styrene oxide	56
cis-stilbene	*cis*-stilbene oxide	39
trans-stilbene	*trans*-stilbene oxide	36
cyclohexane	cyclohexanol	24
	cyclohexanone	4.5
cyclohexanol	cyclohexanone	54
toluene	benzyl alcohol	24
	benzaldehyde	3.2
benzyl alcohol	benzaldehyde	70
	benzoic acid	1.2
tetrahydrofuran	γ-butyrolactone	30

[a] Yield calculated on the basis of oxo complex concentration in 1:1 stoichiometric reaction. [b] 100 − η indicates the unreacted original substance.

The low values of $\Delta H^{\ddagger}$ and large negative values of $\Delta S^{\ddagger}$ clearly support an associative mechanism for the formation of the epoxide either by a concerted (2 + 2) or a nonconcerted (1 + 2) cycloaddition.

Since an epoxidation reaction involves addition of an electrophilic oxygen species to nucleophilic olefins, the olefin geometry and its nucleophilicity are the two most important factors for the formation of one associative intermediate (I). In order to understand the electronic effect in the epoxidation reaction, we have studied the epoxidation of different phenyl-substituted styrenes, viz. 2-methyl-, 3-chloro-, and 4-methoxystyrene. A plot of log of yield with substituted styrene relative to that of styrene (log Y_H), i.e. log Y_X/Y_H, vs σ (substituent constant) (Figure 6) is linear and clearly shows that electron-releasing substituents increase the epoxide yield. This type of plot was reported by Tolman[33] in the oxidation of cyclohexane catalyzed by different phenyl ring substituted porphyrin complexes ([$Fe(T_{4-x}PP)Cl$]). The reaction constant (ρ) determined from the slope of the plot is −0.3. The reaction constant (ρ) reported for the oxidation of different phenyl ring substituted styrenes catalyzed by $(Br_8TPP)Cr^{V}(O)(X)$ was

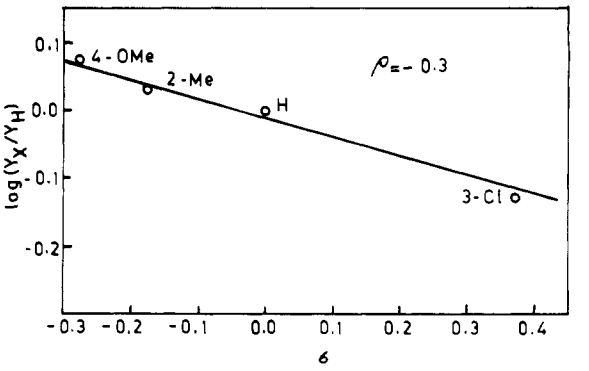

Figure 6. Plot of log Y_X/Y_H vs σ at 30 °C in the oxidation of phenyl-ring-substituted styrene with $Ru^{V}(EDTA)(O)^{-}$ complex in water–dioxane medium.

(33) Nappa, M. J.; Tolman, C. A. *Inorg. Chem.* **1985**, *24*, 4711.

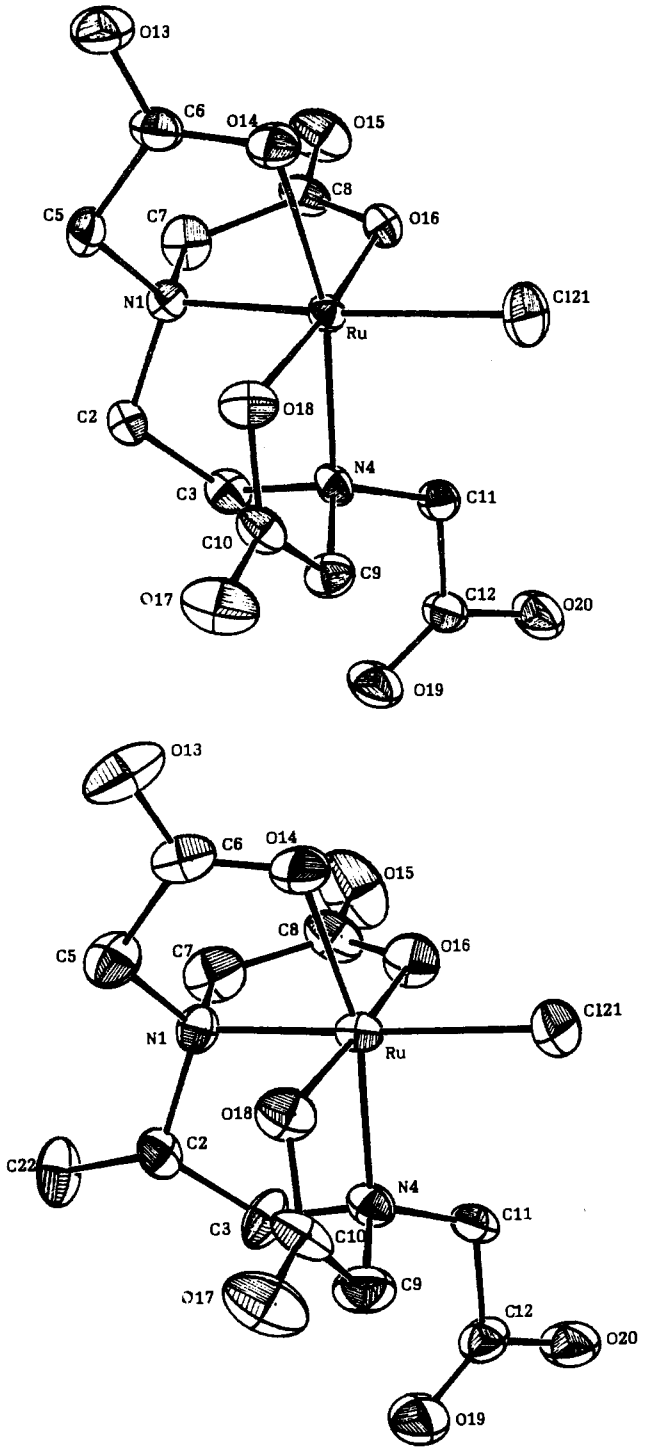

Figure 7. ORTEP diagrams of **1** (a, top) and **2** (b, bottom).

−1.9.[34] The more negative value of ρ of −0.3 obtained in our case reflects a lower electrophilic nature of the oxo oxygen in d^3 Ru^V–oxo complexes **3** and **4** than the d^1 Cr^V–oxo complex.[34] Besides the nucleophilicity of the olefin, the steric effect of the substrates also plays an important role in the epoxidation reaction. Considering both factors, the observed reactivities of the olefins toward epoxidation decrease in the order cyclooctene > cyclohexene > styrene > *cis*- and *trans*-stilbene. Cyclooctene is the most reactive olefin in the series due to its strong nucleophilicity and a more flexible geometry than cyclohexene. Further, the role of electronic and steric effects of the olefin in the epoxidation is clearly indicated by the competitive reaction in a mixture of olefins.

(34) Garrison, J. M.; Osionic, D.; Bruice, T. C. *J. Am. Chem. Soc.* **1989**, *111*, 4960.

Scheme III

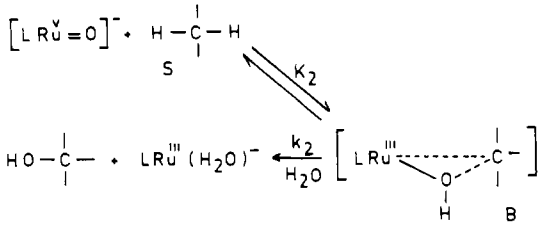

L = EDTA, PDTA. S = Cyclohexane, toluene

In a mixture of cyclohexene and styrene, the former was epoxidized 2.2 times faster than styrene.

Kinetics of Hydroxylation of Cyclohexane and Toluene with $[LRu^V(O)]^-$. The kinetics of the oxidations of cyclohexane and toluene were studied spectrophotometrically by following the same method as followed for the epoxidation of olefins. The reaction rate was found to be first order with respect to the oxo complex concentration and substrate concentration. At high substrate concentration a zero order rate with respect to substrate concentration was observed for both cases. On the basis of the above kinetic results, the mechanism shown in Scheme III is proposed.

On the basis of the mechanism proposed in Scheme III, the following rate expression can be derived:

$$k_{2(\text{obs})} = \frac{k_2 K_2[S']}{1 + K_2[S']} \tag{16}$$

or

$$\frac{1}{k_{2(\text{obs})}} = \frac{1}{k_2} + \frac{1}{k_2 K_2[S']} \tag{17}$$

k_2 values were calculated by using eq 17 and are summarized in Table III.

In the proposed mechanism the oxo oxygens of the complexes $LRu^V{=}O^-$ attack the H–C bond of the cyclohexane or toluene in a equilibrium step to form a transient intermediate "B" through a concerted pathway (Scheme III). Thereafter transfer of an OH group from the metal center to a carbonium ion of the substrate occurs in a rate-determining step to give the corresponding alcohol as a reaction product. Though direct evidence for the formation of intermediate B was not obtained, the kinetic data, however, provide a good fit to the proposed mechanism (Scheme III). To get more information on the mechanism of H–C activation, kinetic isotope effect studies were performed for the hydroxylation of deuterated cyclohexane (C_6D_{12}). The value of k_H^2/k_D^2 observed at 40 °C is 10.5, which is close to that observed for the hydroxylation of tetradeuterated norbornane[35] (k_H/k_D = 11.5).

Jones and Trager[36] had separated the intramolecular isotope effect for cytochrome P-450 hydroxylation of [1,1,1-$^2H_3$]-*n*-octane into a primary effect that lies between 7.3 and 7.9 and the secondary isotope effect between 1.09 and 1.14. The intermolecular isotope effect in our case fits very well with the suggestion of Groves[37] of an O atom rebond mechanism with a highly symmetrical transition state. In the case of the unsymmetrical transition state as observed in the hydroxylation of C_6H_{12} by $KHSO_5$ catalyzed by manganese porphyrins[38] the effect observed is very low at around 2.

The hydroxylations of cyclohexane and toluene were studied at three different temperatures. The rate and activation parameters are presented in Table III. The low ΔH^* values and highly negative values of ΔS^* are in good agreement with the mechanism proposed for the hydroxylation of cyclohexane and toluene. The rate of hydroxylation of the side chain primary cation in toluene is slower than that of the secondary carbon in cyclohexane as expected from the strength of the C–H bond, primary > secondary.

(35) Groves, J. T.; McClusky, G. A.; White, R. E.; Coon, M. J. *Biochem. Biophys. Res. Commun.* **1978**, *81*, 154.
(36) Jones, J. P.; Trager, W. F. *J. Am. Chem. Soc.* **1987**, *109*, 2171.
(37) Groves, J. T.; Nemo, T. E. *J. Am. Chem. Soc.* **1983**, *105*, 6243.
(38) Robert, A.; Meunier, B. *New J. Chem.* **1988**, *12*, 805.

Scheme IV

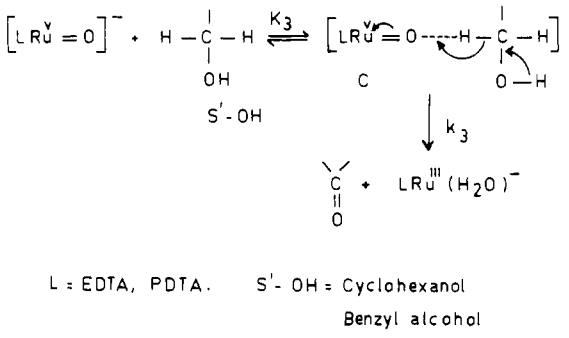

L = EDTA, PDTA. S'-OH = Cyclohexanol, Benzyl alcohol

The reaction with toluene did not give any nuclear hydroxylation products.

Kinetics of Oxidation of Cyclohexanol and Benzyl Alcohol with $LRu^{V}=O^{-}$. The oxidation of cyclohexanol to cyclohexanone and benzyl alcohol to benzaldehyde was studied further, as trace amounts of cyclohexanone and benzaldehyde were obtained as reaction products in the oxidation of cyclohexane and toluene by $LRu^{V}=O^{-}$. The rate of oxidation of the alcohol (cyclohexanol, benzyl alcohol) was first order with respect to the concentration of oxo complex $LRu^{V}=O^{-}$. Increase of alcohol concentration increased the reaction rate, and at high alcohol concentration the reaction rate became independent of alcohol concentration; i.e., saturation in rate was attained. On the basis of the above experimental facts, a mechanism for the oxidation of cyclohexanol to cyclohexanone and benzyl alcohol to benzaldehyde is proposed in Scheme IV, for which the rate expression is given in eqs 11 and 12.

$$k_{3(obs)} = \frac{k_3K_3[S'OH]}{1 + K_3[S'OH]} \quad (18)$$

or

$$\frac{1}{k_{3(obs)}} = \frac{1}{k_3} + \frac{1}{k_3K_3[S'OH]} \quad (19)$$

The values of k_3 calculated by using eq 19 are summarized in Table III.

In the suggested mechanism, the oxo oxygen of $LRu^{V}=O^{-}$ first attacks the C-H bond in alcohol to give rise to an intermediate "C", which in turn rearranges in a rate-determining step to give cyclohexanone or benzaldehyde as the reaction product. The major energetic factor here is the formation of the carbonyl group. The oxidation of cyclohexanol to cyclohexanone and benzyl alcohol to benzaldehyde was studied at three different temperatures, and the rate and activation parameters ($\Delta H^{\ddagger}$ and $\Delta S^{\ddagger}$) are presented in Table III.

Oxidation of the cyclic ether tetrahydrofuran with $LRu^{V}=O^{-}$ was carried out under experimental conditions identical with those described for olefin epoxidation and oxidation of a saturated substrate. The rate and activation parameters are presented in Table III. It is of interest to note that no hydroxylated intermediate of tetrahydrofuran could be detected during the product analysis. Hence, it is assumed that the very reactive γ-hydroxytetrahydrofuran if formed in the reaction mixture during oxidation of tetrahydrofuran with $LRu^{V}=O$ rearranges itself rapidly to the stable γ-butyrolactone as the ultimate reaction product.

Registry No. $K[Ru^{III}(EDTA\text{-}H)Cl]$, 76095-13-1; $K[Ru^{III}(PDTA\text{-}H)Cl]$, 141271-84-3; $K[Ru^{III}(EDTA\text{-}H)Cl]\cdot 2H_2O$, 141248-95-5; $K[Ru^{III}(PDTA\text{-}H)Cl]\cdot 0.5H_2O$, 141271-82-1; $Ru^{III}(EDTA)(OH)^{2-}$, 66844-68-6; $Ru^{III}(PDTA)(OH)^{2-}$, 141248-96-6; $K[Ru^{V}=O(EDTA)]\cdot 3H_2O$, 141248-97-7; $K[Ru^{V}=O(PDTA)]\cdot 3H_2O$, 141271-83-2; cyclohexene, 110-83-8; cyclooctene, 931-88-4; styrene, 100-42-5; *cis*-stilbene, 645-49-8; *trans*-stilbene, 103-30-0; cyclohexane, 110-82-7; tetrahydrofuran, 109-99-9; 2-Me-styrene, 611-15-4; 3-Cl-styrene, 2039-85-2; 4-MeO-styrene, 637-69-4; cyclohexene oxide, 286-20-4; cyclooctene oxide, 286-62-4; styrene oxide, 96-09-3; 2-Me-styrene oxide, 2783-26-8; 3-Cl-styrene oxide, 20697-04-5; 4-MeO-styrene oxide, 6388-72-3; *cis*-stilbene oxide, 1689-71-0; *trans*-stilbene oxide, 1439-07-2; cyclohexanol, 108-93-0; cyclohexanone, 108-94-1; benzyl alcohol, 100-51-6; benzaldehyde, 100-52-7; γ-butyrolactone, 96-48-0.

Supplementary Material Available: Tables of positional parameters, general displacement parameter expressions, bond distances, least-squares planes, and torsional angles (18 pages); listings of observed and calculated structure factors (20 pages). Ordering information is given on any current masthead page.

Contribution from the Department of Chemistry and Laboratory for Molecular Structure and Bonding, Texas A&M University, College Station, Texas 77843-3255, and Department of Chemistry, University of Costa Rica, Ciudad Universitaria, Costa Rica

Mononuclear-Dinuclear Equilibrium for the Pyridine Adducts of Chromium(II) Saccharinates

Nuria M. Alfaro,[1a] F. Albert Cotton,*[1b] Lee M. Daniels,[1b] and Carlos A. Murillo*[1a]

Received January 17, 1992

The azeotropic removal of water by pyridine from $[Cr(Sac)_2(H_2O)_4]\cdot 2H_2O$, Sac = the anion of saccharine, gives a solution with a mixture of a mononuclear and dinuclear chromium(II) saccharinate, the relative concentration of which varies with changes in temperature. Appropriate workup of the pyridine solution has provided crystals of $[Cr_2(Sac)_4(py)_2]\cdot 2py$ (**1**) and $[Cr(Sac)_2(py)_3]\cdot 2py$ (**2**). Both compounds have been characterized by X-ray crystallography at −60 °C. The chromium-to-chromium bond length in **1** (2.5911 (8) Å) is one of the longest ones known of any dichromium(II) dimer. Compound **1** crystallizes in the monoclinic space group *Ia*, with a = 11.705 (2) Å, b = 21.868 (2) Å, c = 20.649 (2) Å, β = 98.87 (1)°, V = 5222 (2) Å^3, and Z = 4. The structure of the five-coordinated compound **2** is bipyramidal and is easily envisioned as the result of breaking the metal-to-metal bond in **1** and replacing the O-bonded saccharinate groups by pyridine molecules. Compound **2** crystallizes in the monoclinic space group $C2/c$, with a = 13.347 (2) Å, b = 26.134 (2) Å, c = 11.802 (2) Å, β = 110.541 (7)°, V = 3855 (1) Å^3, and Z = 4. Both compounds possess interstitial pyridine molecules that occupy channels formed in the crystal. Under appropriate conditions **1** and **2** are reversibly interconvertable both in the solid state and in pyridine solution.

Introduction

The chemistry of chromium(II) is very rich in mononuclear six-coordinated compounds, most of them having the high-spin electronic configuration. One point of particular interest has been the Jahn-Teller distortion exhibited by these compounds.[2] There is also a more limited number of four-coordinated species, either nearly planar or tetrahedral,[3] and a few reports of three- and five-coordinated compounds.[4] To our knowledge, there is only

(1) (a) University of Costa Rica. (b) Texas A&M University.
(2) Cotton, F. A.; Wilkinson, G. *Advanced Inorganic Chemistry*, 5th ed.; John Wiley & Sons: New York, 1988; Chapter 18, pp 683-686.
(3) See for example: (a) Bradley, D. C.; Hursthouse, M. B.; Newing, C. W.; Welch, A. J. *J. Chem. Soc., Chem. Commun.* **1972**, 567. (b) Cotton, F. A.; Falvello, L. R.; Schwotzer, W.; Murillo, C. A.; Valle-Bourrouet, G. *Inorg. Chim. Acta* **1991**, *190*, 89 and references cited therein.

0020-1669/92/1331-2718$03.00/0